J Solid State Electrochem (2007) 11:619–629
DOI 10.1007/s10008-006-0208-x

ORIGINAL PAPER

CO_2 corrosion inhibition by hydroxyethyl, aminoethyl, and amidoethyl imidazolines in water–oil mixtures

W. Villamizar · M. Casales · J. G. Gonzalez-Rodriguez · L. Martinez

Received: 4 March 2006 / Revised: 28 July 2006 / Accepted: 28 July 2006 / Published online: 12 October 2006

Abstract The corrosion behavior of hydroxyethyl, amino ethyl and amid ethyl imidazolines corrosion inhibitors was evaluated by using potenthiodynamic polarization curves, linear polarization resistance, and electrochemical impedance spectroscopy techniques. Solutions included deaerated 3% NaCl, 3% NaCl+diesel saturated with CO_2 at 50 °C with and without inhibitors. Regardless of the presence of diesel, the corrosion rate was decreased with the addition of the inhibitors, but the time to reach a steady state was longer than when the oily part, i.e., diesel, was present. In the absence of the oily part, the impedance results showed that the film formed was porous, allowing the electrolyte to diffuse through it and corrode the metal. When the oily part was present, the film formed was much more stable, not porous, and did not allow the electrolyte to corrode the sample. The most efficient inhibitor was the amid ethyl imidazoline, whereas the least efficient was the hydroxyethyl imidazoline, because the film formed by the former was much more stable from the beginning of the test.

Keywords CO_2 corrosion · Imidazolines · Diesel · Electrochemical techniques

W. Villamizar · M. Casales · L. Martinez
UNAM_Centro de Ciencias Físicas,
Av. Universidad S/N, Col. Chamilpa,
62210 Cuernavaca, Mor, Mexico

J. G. Gonzalez-Rodriguez (✉)
UAEM-CIICAp,
Av. Universidad 1001, Col. Chamilpa,
62210 Cuernavaca, Mor, Mexico
e-mail: ggonzalez@uaem.mx

Introduction

Oilfield corrosion manifests itself in several forms, among which CO_2 corrosion (sweet corrosion) and hydrogen sulfide (H_2S) corrosion (sour corrosion) in the produced fluids and corrosion by oxygen dissolved in water injection are by far the most prevalent forms of attack found in oil and gas production [1].

The addition of corrosion inhibitors is a standard practice in oil and gas production systems to control the internal corrosion of carbon steel structures. Nitrogen-based organic inhibitors, such as imidazolines or their salts, have been successfully used in these applications even without an understanding the inhibition mechanism [2–4]. The corrosion inhibition of organic compounds is related to their adsorption properties. Adsorption depends on the nature and state of the metal surface, on the type of corrosive environment, and on the chemical structure of the inhibitor [5]. Studies report that the adsorption of the organic inhibitors mainly depends on some physico-chemical properties of the molecule, related to its functional groups, to the possible steric effects, and to the electronic density of donor atoms; adsorption is also suppose to depend on the possible interaction of the π-orbitals of the inhibitor with the d-orbitals of the surface atoms, which induce greater adsorption of the inhibitor molecules onto the surface of metal, leading to the formation of a corrosion-protection film [6].

Different derivatives from imidazolines are employed as steel corrosion inhibitors. Even though they have been specially employed in the oil industry, only recently have many studies been undertaken to understand how they work [7–13]. These works imply some key questions regarding the structure–performance relationships of imidazolines, the role of the hydrocarbon chain head group and pendant group in

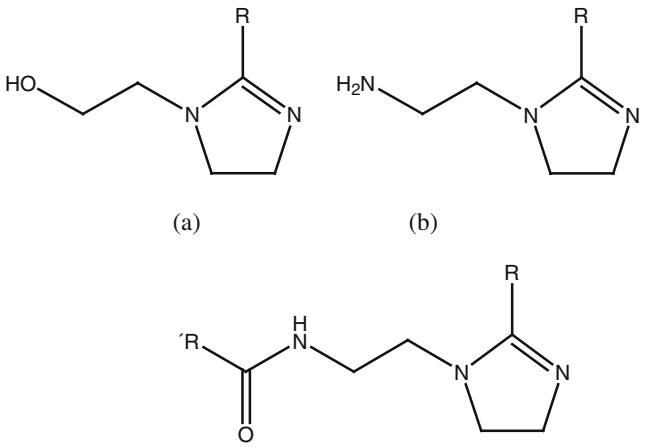

Fig. 1 Molecular formulas of the imidazolines used: **a** hydroxyethyl (HEI-18b), **b** aminoethyl (AEI-18), and **c** amidoethyl (AMEI-18) imidazolines. *R* and *R′* alkyl chain of C_{17}

film formation, the thickness of the imidazoline film, the stability of the imidazoline group and the solution composition, and the hydrolysis of imidazoline, among others.

The purpose of this paper is to evaluate the behavior of hydroxyethyl, aminoethyl, and amidoethyl imidazolines as corrosion inhibitors in the CO_2 corrosion of 1018 carbon steel using an electrochemical technique in an environment containing NaCl, CO_2, and diesel to simulate environments found in the transport of crude oil.

Experimental

Test material

Three standard identical "finger-electrodes," fabricated from 1018-type carbon steel, were used. Before testing, the electrode was polished with 600 grit silicon carbide emery paper and then cleaned with alcohol, acetone, and distilled water.

Test solution

Three types of commercial imidazolines, namely, hydroxyethyl, aminoethyl, and amidoethyl imidazolines, were used in this study (Fig. 1), with some of their properties given in Table 1. The inhibitors were dissolved in pure 2-propanol. The concentration of the inhibitor used in this work was 20 ppm and the temperature was kept at 50 °C. Before applying the inhibitor, a solution containing 3% NaCl was prepared. The testing solution consisted of either pure 3% NaCl solution or 90% of this solution+10% diesel emulsion, which was heated, deaerated with nitrogen gas, and CO_2-saturated for 2 h, and then the inhibitor was added. Continuous stirring was used and CO_2 was bubbled during the tests.

Electrochemical measurements

Continuous electrochemical corrosion was monitored using three identical electrode corrosion probes. Electrochemical techniques employed included potentiodynamic polarization curves, linear polarization resistance (LPR), and electrochemical impedance spectroscopy (EIS) measurements. Polarization curves were recorded at a constant sweep rate of 1 mV/s and the scanning range was from −300 to +300 mV with respect to the open circuit potential, E_{corr}. Measurements were obtained by using a conventional three-electrode glass cell, with two graphite electrodes symmetrically distributed and a saturated calomel electrode as a reference electrode with a Lugging capillary bridge. Inhibition efficiencies [*E*(%)] were determined from the corrosion current densities calculated by the Tafel extrapolation method according to the following equation:

$$E(\%) = \frac{i_b - i_j}{i_b} \times 100 \quad (1)$$

where i_b is the corrosion rate without inhibitor and i_i the corrosion rate in the solution with inhibitor.

LPR measurements were carried out by polarizing the specimen from +10 to −10 mV with respect to E_{corr}, at a scanning rate of 1 mV/s. Inhibition efficiencies [*E*(%)] were determined according to the following equation:

$$E(\%) = \frac{R_{p,i} - R_{p,b}}{R_{p,i}} \times 100 \quad (2)$$

where $R_{p,b}$ is the LPR without inhibitor and $R_{p,i}$ is the LPR with inhibitor. EIS tests were carried out at E_{corr} by using a signal with an amplitude of 10 mV and a frequency interval

Table 1 Electrochemical parameters for 1018 carbon steel exposed to NaCl 3% solution saturated with CO_2 with addition of the different types of imidazoline

Inhibitor	E_{corr} (V)	i_{corr} (μA cm^{-2})	b_a (mV/decade)	b_c (mV/decade)	V_{corr} (mpy)	*E* (%)
Blank	−0.730±0.004	273.94±64.66	63.57±2.37	−872.72±129	125.33±29.59	
HEI-18	−0.638±0.004	123.65±3.84	53.53±0.95	−476.04±32.63	56.57±1.71	54.8
AEI-18b	−0.631±0.002	109.03±17.11	37.47±10.6	−355.93±65.02	49.88±7.83	60.2
AMEI-18	−0.719±0.001	176.07±3.51	70.59±2.16	−458.09±23.23	80.55±1.61	35.7

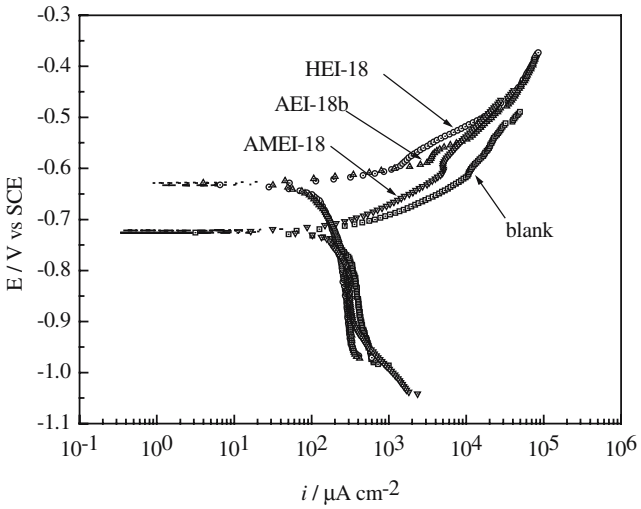

Fig. 2 Polarization curves for 1018 carbon steel with the different imidazolines exposed to 3% NaCl solution

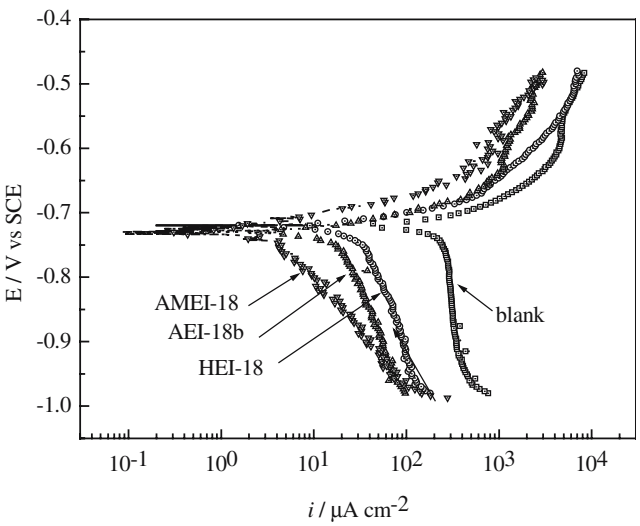

Fig. 3 Polarization curves for 1018 carbon steel with the different imidazolines exposed to 3% NaCl+diesel solution. **a** HEI-18, **b** AEI-18b, and **c** AMEI-18

of 0.1–100 kHz. An Applied Corrosion Monitoring potentiostat controlled by a desktop computer was used for the LPR tests and polarization curves, whereas for the EIS measurements, a model PC4 300 Gamry potentiostat was used. All the tests were carried out at 50 °C and lasted 9 h.

Results and discussion

Polarization curves

Figure 2 shows the polarization curves for carbon steel in 3% NaCl saturated with CO_2 with the addition of 20 ppm of inhibitors. These curves show that both the cathodic and anodic current densities were lowered by the addition of the imidazolines, although this effect was minimal with the addition of the AMEI-18-type imidazolines. With the addition of the AEI-18b inhibitor, a significant displacement of the E_{corr} valued in the positive direction was produced. The greatest inhibition efficiency, i.e., 60.2%, was recorded for the AEI-18b-type imidazolines, whereas the smallest value was for the AMEI-18-type imidazoline, with an efficiency value of 35.7%. The inhibitors did not affect the cathodic current density, but only the anodic branch, indicating that they act as anodic inhibitors. The electrochemical parameters, corrosion rate, and efficiency values for the three imidazolines are shown in Table 1. It is clear that the imidazolines AEI-18b and HEI-18 gave a better inhibiting effect.

Polarization curves for the 3% NaCl+diesel solution are shown in Fig. 3. In general terms, the corrosion current density values, i_{corr}, are lowered with respect to the solution without diesel, but the E_{corr} values are now very close to each other, around −700 mV. Once again, the addition of the inhibitors decreases both the anodic and cathodic current density values with respect to the uninhibited solution, especially with the AMEI-18-type inhibitor. The electrochemical parameters and corrosion current density and efficiency values are shown in Table 2. In this case, the least efficient inhibitor was HEI-18, with an efficiency value of 87.2%, and, once again, the most efficient inhibitor was AMEI-18, with an efficiency value of 98.4%. The inhibitors did affect both the anodic and cathodic current densities when diesel was present, so in this case, they acted as mixed inhibitors.

Table 2 Electrochemical parameters for 1018 carbon steel exposed to NaCl 3%+diesel solution saturated with CO_2 with addition of the different types of imidazoline

Inhibitor	E_{corr} (V)	i_{corr} (μA cm^{-2})	b_a (mV/decade)	b_c (mV/decade)	V_{corr} (mpy)	E(%)
Blank	−0.720±0.006	258.5±33.8	82.7±15.9	−1,536.0±131.4	118.1±15.4	
HEI-18	−0.722±0.008	33.0±3.1	70.9±21.7	−388.6±48.5	15.1±1.4	87.2
AEI-18b	−0.729±0.007	19.4±1.6	69.7±18.6	−358.2±26.5	8.9±0.7	92.5
AMEI-18	−0.735±0.010	4.0±0.3	54.5±6.3	−160.4±8.2	1.8±0.1	98.4

LPR results

The changes in the LPR values, R_p, for the 3% NaCl and 3% NaCl+Diesel (oil) with and without the addition of the different inhibitors are given in Fig. 4. During the first 2 h, before the addition of the inhibitors, the R_p values were slightly higher for the solution without diesel except for the HEI-18 type inhibitor. When the inhibitors were added, the R_p values for the solution with diesel increased up to six orders of magnitude with respect to the uninhibited solution, whereas for the solution without diesel these values increased only one order of magnitude. This means that the corrosion rates for the solutions with diesel were several orders of magnitude lower than those obtained without diesel, indicating that the oily part, i.e., diesel, helped to increase the inhibitor efficiency. The time to decrease the corrosion rate was longer for the HEI-18 inhibitor than that for the AEI-18b and AMEI-18 inhibitors. The time to reach a steady state in the corrosion rate was much faster when diesel was present than when it was not. The highest efficiency obtained when diesel was present was for inhibitor AMEI-18 (amidoethyl imidazoline), 98%, whereas the least efficient was inhibitor HEI-18b (hydroxyethyl imidazoline), 89%. These data tell us the important role of the oily part of the emulsion to form a protective film more rapidly and, thus, reduce the corrosion rate, because these inhibitors are oil-soluble and not water-soluble. This variation in corrosion rate values can be described by the different solubilities and the hydrophobic characters of the imidazolines in the two environments. In fact, imidazoline HEI-18 is not soluble in water, imidazoline AEI-18 is dispersible in water, and imidazoline AMEI-18 is the most hydrophobic of all of them due to the presence of two large alkyl groups.

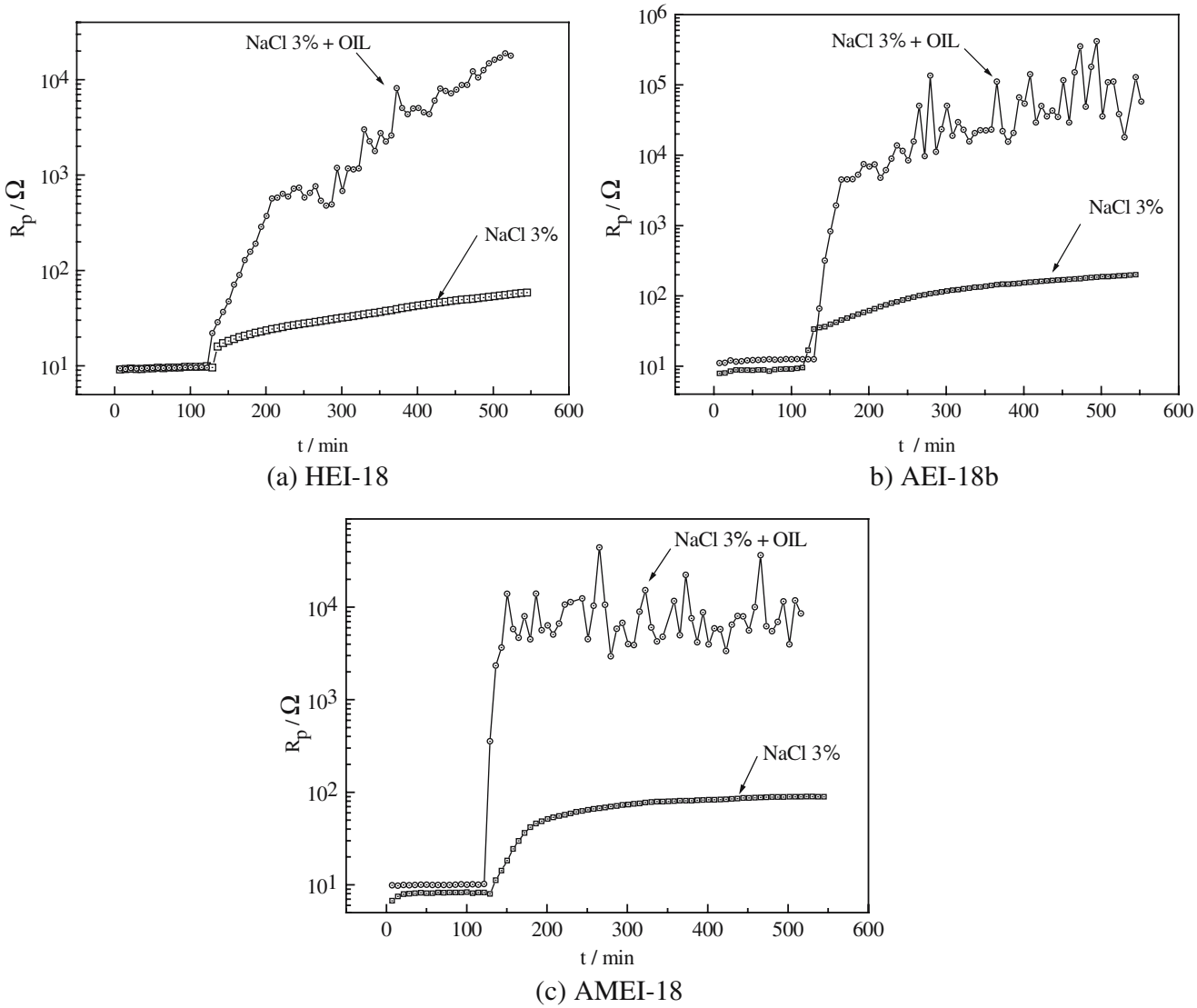

Fig. 4 Variation of the LPR (R_p) with time for 1018 carbon steel exposed to 3% NaCl and 3% NaCl+diesel solutions with the different types of imidazolines

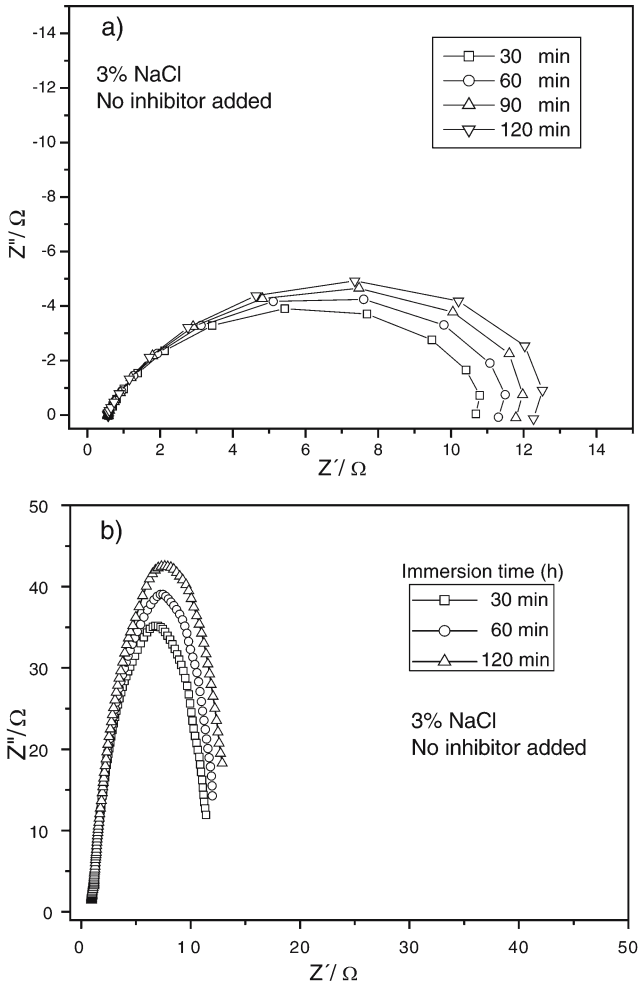

Fig. 5 Nyquist diagrams for uninhibited **a** 3% NaCl and **b** 3% NaCl+diesel solutions. *Symbols* represent experimental values, *solid lines* are the predicted values

EIS results for uninhibited solutions

The Nyquist data for the uninhibited 3% NaCl without and with diesel are given in Fig. 5. This behavior is typical for solid metal electrodes that show frequency dispersion of the impedance data [14]. Electrically equivalent circuits are generally used to model the electrochemical behavior and calculate the parameters of interest, such as electrolyte resistance (R_s), charge transfer resistance (R_{ct}), and double-layer capacitance (C_{dl}) [15]. When a nonideal frequency response is present, it is commonly accepted to employ distributed circuit elements in an equivalent circuit. The most widely used is constant phase element (CPE), which has a noninteger power dependence on the frequency. The impedance of a CPE is described by the expression:

$$Z_{CPE} = Y^{-1}(iw)^{-n} \quad (3)$$

where Y is a proportional factor, i is $\sqrt{-1}$, w is $2\pi f$, and n has the meaning of a phase shift [14]. Often, a CPE is used in a model in place of a capacitor to compensate for nonhomogeneity in the system.

The impedance spectra for both solutions exhibited, in all cases, a single (capacitive-like) semicircle and then only one CPE, which can be modeled as an electric equivalent circuit given in Fig. 6. The fitting parameters for both solutions are given in Tables 3 and 4, respectively, and they appear as solid lines in Fig. 5. The R_{ct} values when diesel is present are slightly higher than when diesel is absent, as shown in Fig. 7, indicating that the oily part, without inhibitor, does not form a protective film. This is because the inhibitor is not miscible in water, so it will not reach the whole metal surface to form a continuous protective layer. The increase in the proportional factor Y of CPE has been related to the growing area of an iron carbonate deposit on the surface of the samples. At 50 °C, these scales are porous and nonhomogeneous, allowing the access of the corroding solution to the base material. These scales, however, seem to provide some corrosion protection to the metal beneath them by restricting the mass transfer of reactants and products between the bulk solution and the metal, which is represented by an increase in the corresponding R_{ct} values. On the other hand, there is no evidence of the formation of a protective $FeCO_3$ film because there is only one capacitive loop in the EIS Nyquist plots [16]. This could be due to the formation of a porous thin layer of $FeCO_3$ with a resistance that is much smaller than the charge transfer resistance, R_{ct}. The semicircle representing the $FeCO_3$ film merges with the charge

Table 3 Circuit parameters for 1018 carbon steel in uninhibited 3% NaCl solution

Time (min)	R_s (Ω)	R_{ct} (Ω)	Y_{dl} (ohms×10^{-6} s^n)	n
30	0.57002	10.68	0.0046	0.79
60	0.56734	11.45	0.0048	0.80
120	0.56373	12.68	0.00514	0.81

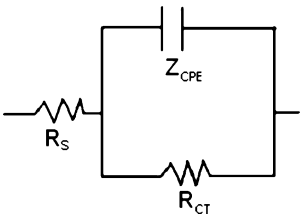

Fig. 6 Equivalent circuit used to represent the impedance results for uninhibited 3% NaCl and 3% NaCl+diesel solutions

Table 4 Circuit parameters for 1018 carbon steel in uninhibited 3% NaCl+diesel solution

Time (min)	R_s (Ω)	R_{ct}(ohms cm^{-2})	Y_{dl}(ohms×10^{-6} s^n)	n
30	8.50	12	459	0.77
60	8.45	14	510	0.77
120	8.64	16	539	0.78

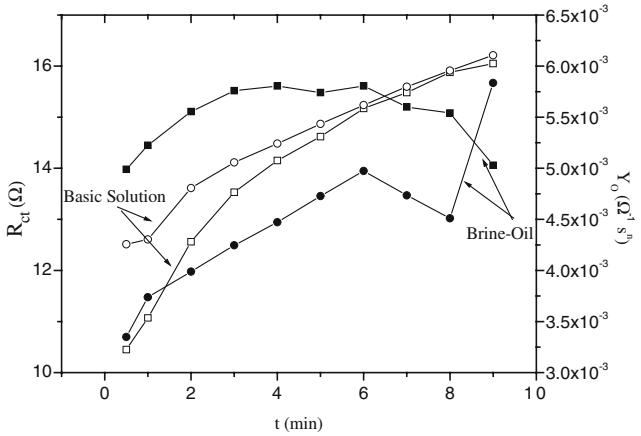

Fig. 7 R_{ct} and Y_0 for uninhibited solutions: *Squares* represent R_{ct} and *circles* represent Y_0; 3.5% for NaCl (*open symbols*) and 3.5% NaCl+ diesel solutions (*filled symbols*)

transfer loop, and hence, the EIS data are described by a simple capacitive semicircle [17].

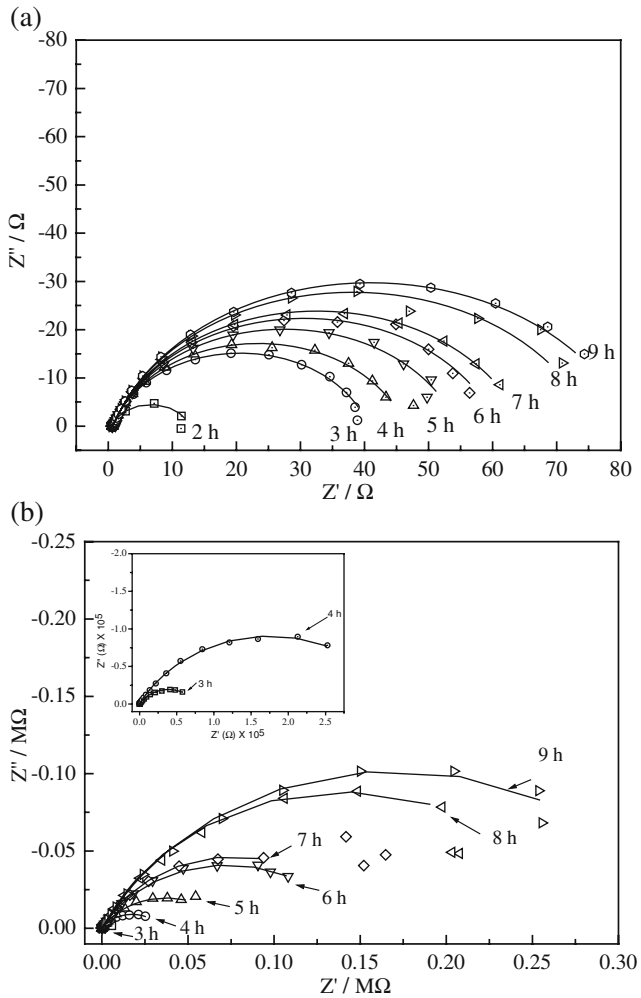

Fig. 8 Nyquist diagrams for carbon steel at different immersion times in inhibited 3% NaCl solution using inhibitor HEI-18: **a** without diesel and **b** with diesel. *Symbols* are experimental values, *solid lines* are the calculated values

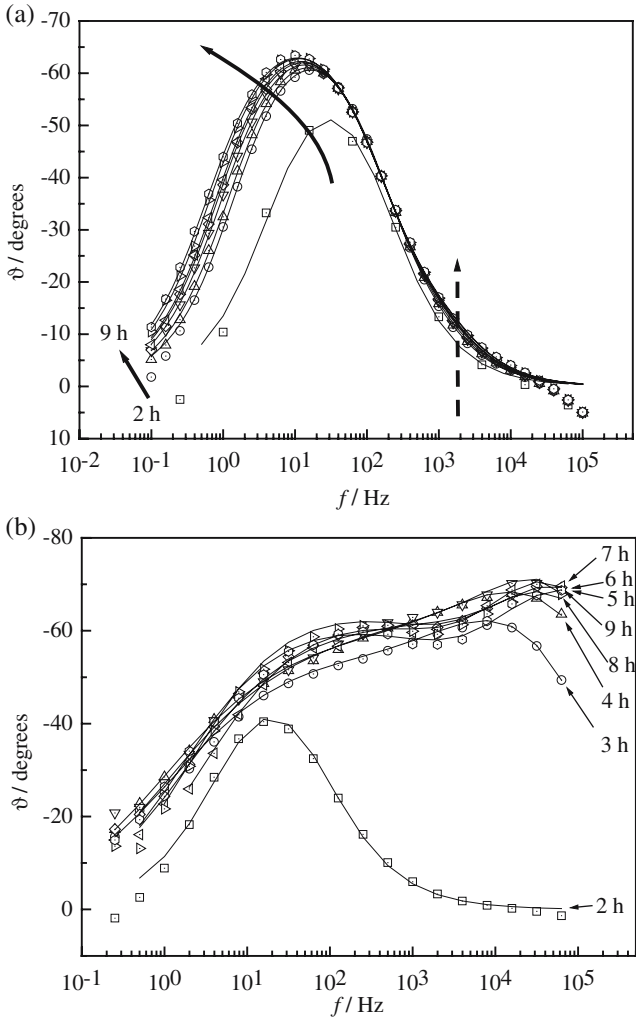

Fig. 9 Bode diagrams for carbon steel at different immersion times in inhibited 3% NaCl solution using inhibitor HEI-18: **a** without diesel and **b** with diesel. *Symbols* are experimental values, *solid lines* are the calculated values

EIS results for inhibited solutions

Inhibitor HEI-18

Experimental impedance spectra, for the solution with and without the oily part, after the addition of inhibitor HEI-18 at different exposure times are shown in Fig. 8a and b, respectively. The magnitude of the impedance increases continuously with time for both solutions. All experimental spectra have a depressed semicircular shape in the complex impedance plane, with the center under the real axis. The

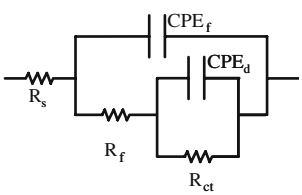

Fig. 10 Equivalent circuit used to interpret the impedance result for inhibited solutions

Table 5 Circuit parameters (time, R_s, R_{ct}, $Y=Y_f+Y_d$ and n) for sample 1018 carbon steel exposed to 3% NaCl solution with inhibitor AEI-18 (hydroxyethyl imidazoline)

t (h)	R_s (Ω)	CPE_f		R_f (Ω)	CPE_d		R_{ct} (Ω)
		Y_f (Ω^{-1} s^n)×10^{-3}	n		Y_d (Ω^{-1} s^n)×10^{-3}	n	
2	0.555	–	–	–	4.99	0.809	13.08
3	0.580	1.48	0.808	0.94	2.80	0.790	57.68
4	0.669	1.11	0.816	0.64	3.27	0.783	68.92
5	0.586	1.06	0.815	0.58	3.19	0.781	80.66
6	0.587	1.07	0.812	0.60	3.08	0.778	93.49
7	0.590	1.09	0.809	0.66	2.92	0.779	107.2
8	0.607	1.06	0.812	0.74	2.89	0.777	119.6
9	0.609	1.07	0.810	0.79	2.86	0.776	130.00

magnitude of the impedance without diesel is still within the order of magnitude compared to the same solution without inhibitor (Fig. 8a) but with the oily part, the impedance magnitude is up to five orders of magnitude higher than the impedance obtained with diesel but without inhibitor (Fig. 8b). This is expected because the inhibitor used was oil-soluble, and thus, the inhibitor would be transported to the surface when the oily part was present. The calculated efficiency for HEI-18 inhibitor by using Eq. 2 after 9 h of immersion time was 80.04 and 99.99% for the solution without and with the oily part, respectively. Thus, it seems that the presence of the oily phase has an effect of coadsorption of the inhibitor on the substrate to improve the inhibitor performance.

Figure 9 shows the corresponding Bode plot for the two test solutions. Once the inhibitor is added to the 3.5% NaCl solution, the Bode phase broadens at a low frequency but does not show a clearly resolved time constants at higher frequencies as exposure time increases. The broadening and slight asymmetry in the Bode plots suggests a second time constant, as is often the case for a porous inhibitor film. When the oily part is present, significant changes are noted. The Bode plot, Fig. 9b, clearly shows the presence of two distinct time constants. These new time constants at higher frequencies relate to the formation of a film on the metal due to the presence of the inhibitor [1, 2] and the effect of coadsorption of the oily phase. As shown in Fig. 9a, the position of the peak at low frequencies shifts towards low frequency values as immersion time increases. However, the peaks for the 3% NaCl+diesel mixture remain unchanged with the immersion time, but the peak height changes as the exposure time elapses. In addition, the peak's height indicates a more capacitive response of the film. Different equivalent circuits have been established to interpret the impedance behavior of coated electrodes with film inhibitors (imidazolines) [1–3, 5–8]. The equivalent circuit shown in Fig. 10 was used to describe the electrochemical process in the presence of the inhibitor for both testing solutions.

For metal electrodes without coating, the diameter of the high-frequency semicircle is treated as the charge transfer resistance R_{ct}. However, for coated electrodes, the high-frequency capacitive loop is related to the barrier and properties of the coating. In the equivalent circuit in Fig. 10, R_s, R_{ct}, and CPE_d have the same physical meanings as in Fig. 6, CPE_f represents the capacitance of the film and R_f represents the resistance of the film, which reflects the protective properties of the film. In this case, $R_f \ll R_{ct}$, hence $Y=Y_f+Y_d \sim Y_d$. The fitting parameters obtained using the electrical circuit shown in Fig. 10 are presented in Tables 5 and 6 as an example for inhibitor HEI-18 (hidroxyethil imidazoline) without and with the addition of diesel. The fitting curves are presented in Figs. 8 and 9 as solid lines for each spectrum, observing an optimum fit with the model for all experimental data, with an estimated error of 3% in all cases.

Table 6 Circuit parameters (time, R_s, R_{ct}, $Y=Y_f+Y_d$ and n) for 1018 carbon steel exposed to 3% NaCl+diesel solution with inhibitor AEI-18 (hydroxyethyl imidazoline)

t (h)	R_s (Ω)	CPE_f		R_f (Ω)	CPE_d		R_{ct} (Ω)×10^4
		Y_f (Ω^{-1} s^n)×10^{-6}	n		Y_d (Ω^{-1} s^n)×10^{-5}	n	
2							
3	1.83	2.493	0.93	36.97	4.043	0.56	0.849
4	1.61	3.439	0.88	219.5	2.380	0.56	0.835
5	1.77	1.263	0.93	147.4	1.385	0.63	1.786
6	2.27	0.719	0.98	84.09	1.220	0.65	1.935
7	1.86	1.256	0.91	413.4	0.604	0.70	1.665
8	2.08	1.360	0.89	877.9	0.460	0.71	2.212
9	1.49	1.636	0.87	3,231	0.329	0.73	3.340

Inhibitor AEI-18

Experimental impedance spectra, for the solution with and without the oily part, after addition of inhibitor AEI-18 at different exposure times are shown in Fig. 11a and b, respectively. The magnitude of the impedance increases continuously with time for both solutions. All experimental spectra have a depressed semicircular shape in the complex impedance plane, with the center under the real axis. The magnitude of the impedance without diesel is still within the same order of magnitude compared to the same solution without inhibitor (Fig. 11a), but with the oily part, the impedance magnitude is up to five orders of magnitude higher than the impedance obtained with diesel but without inhibitor (Fig. 11b). This is expected because the inhibitor used was oil-soluble, and thus, the inhibitor would be transported to the surface when the oily part was present. The calculated efficiencies for AEI-18 inhibitor after 9 h of immersion time were 87.65 and 99.96% for the solution with and without the oily part, respectively. Thus, once again, it seems that the presence of the oily phase has an effect of coadsorption of the inhibitor on the substrate, which helps to improve the performance of the inhibitor.

Figure 12a,b shows the corresponding Bode plot for the same experimental data in the log f vs θ format for both solutions. As in the case of inhibitor HEI-18, the Bode phase broadens at low frequencies but does not show clearly resolved time constants at a higher frequencies as time elapses. Similar to the inhibitor HEI-18, the broadening and slight asymmetry in the bode-phase plots is indicative of a second time constant. When the oily phase is present in the solution, significant changes are noted. The bode plot in Fig. 11b clearly shows the presence of two time constants. As shown in Fig. 11a, the position of the peak at low frequencies is shifted towards low f as the

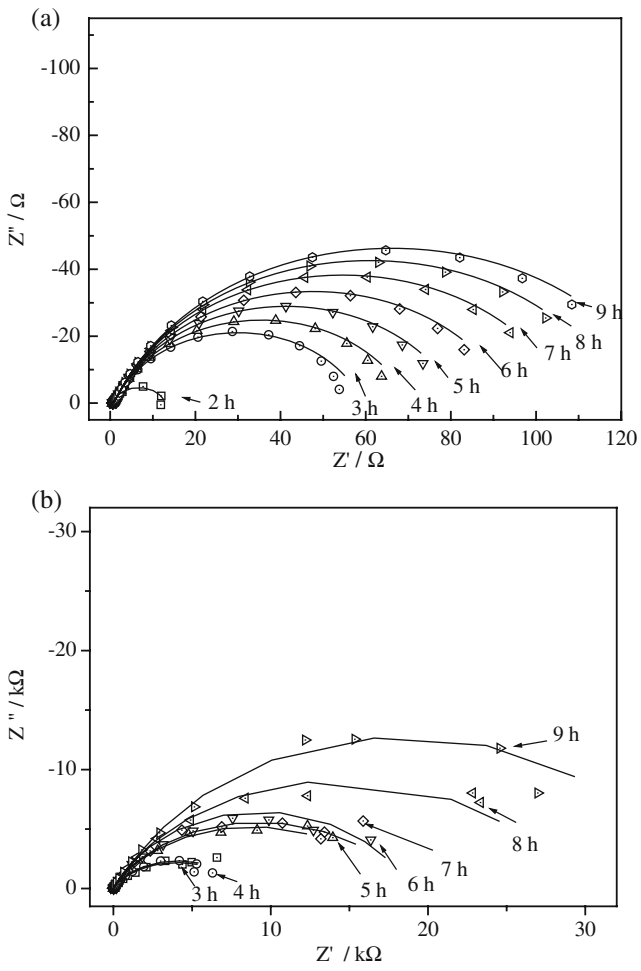

Fig. 11 Nyquist diagrams for carbon steel at different immersion times in inhibited 3% NaCl solution using inhibitor AEI-18: **a** without diesel and **b** with diesel. *Symbols* are experimental values, *solid lines* are the calculated values

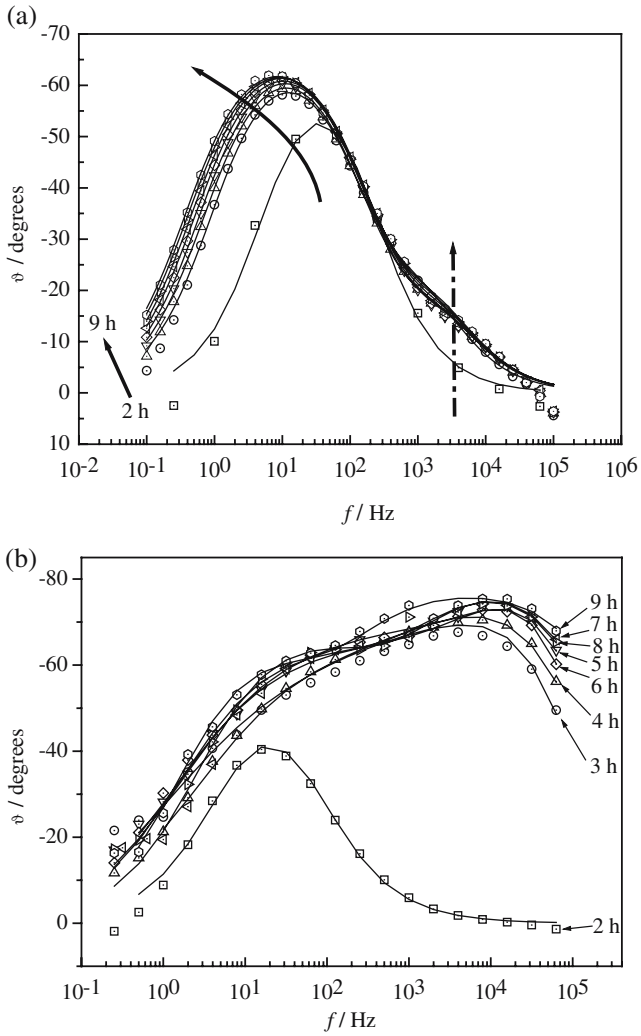

Fig. 12 Bode diagrams for carbon steel at different immersion times in inhibited 3% NaCl solution using inhibitor AEI-18: **a** without diesel and **b** with diesel. *Symbols* are experimental values, *solid lines* are the calculated values

immersion time increases, unlike the peaks for the solution with diesel, which remain constant. The equivalent circuit shown in Fig. 10 was used to describe the electrochemical process in the presence of inhibitor AEI-18 for both solutions. The fitting of curves are shown in Fig. 11a,b and Fig. 12a,b as solid lines for each spectrum, observing an optimum fit with the model for all experimental data, with an estimated error of 3% in all cases.

Inhibitor AMEI-18

Experimental impedance spectra, for the solution with and without the oily part, after the addition of inhibitor AMEI-18 at different exposure times are shown in Fig. 13a,b, respectively.

The magnitude of the impedance increases continuously with time for both solutions. All experimental spectra have a depressed semicircular shape in the complex impedance plane, with the center under the real axis. The magnitude of the impedance without diesel is still within the order of magnitude compared to the same solution without inhibitor (Fig. 13a), but with the oily part, the impedance magnitude is up to five orders of magnitude higher than the impedance obtained with diesel but without inhibitor (Fig. 13b). This is expected because the inhibitor used was oil-soluble, and thus, the inhibitor would be transported to the surface when the oily part was present. The calculated efficiencies for AMEI-18 inhibitor after 9 h of immersion time were 70.62 and 99.99% for the solution with and without the oily part, respectively. Thus, once again, it seems that the presence of the oily phase has an effect of coadsorption of the inhibitor on the substrate that improved the performance of the inhibitor but was higher compared with inhibitors HEI-18 and AEI-18b.

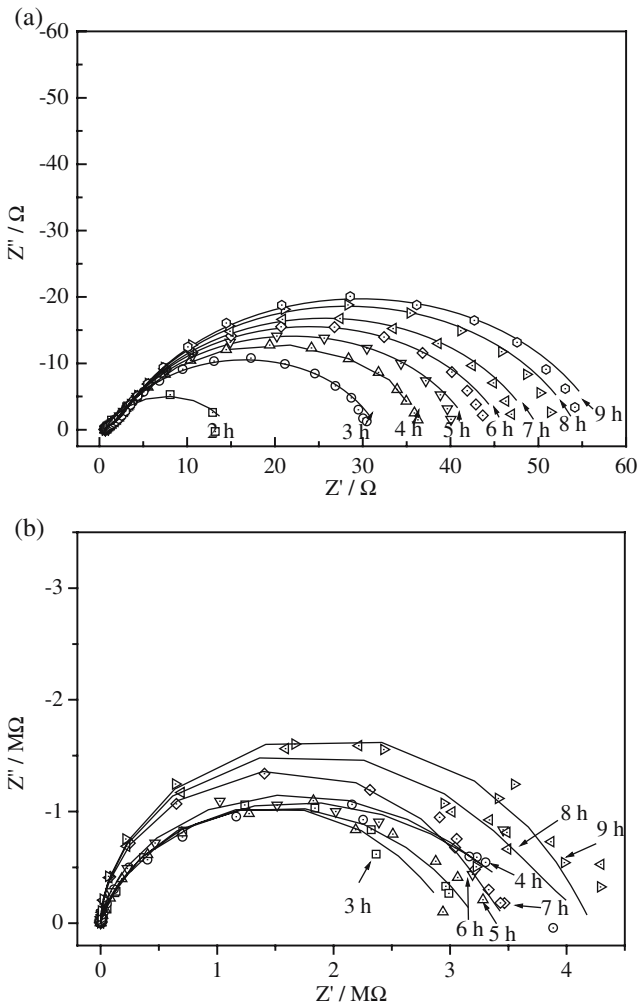

Fig. 13 Nyquist diagrams for carbon steel at different immersion times in inhibited 3% NaCl solution using inhibitor AMEI-18: **a** without diesel and **b** with diesel. *Symbols* are experimental values, *solid lines* are the calculated values

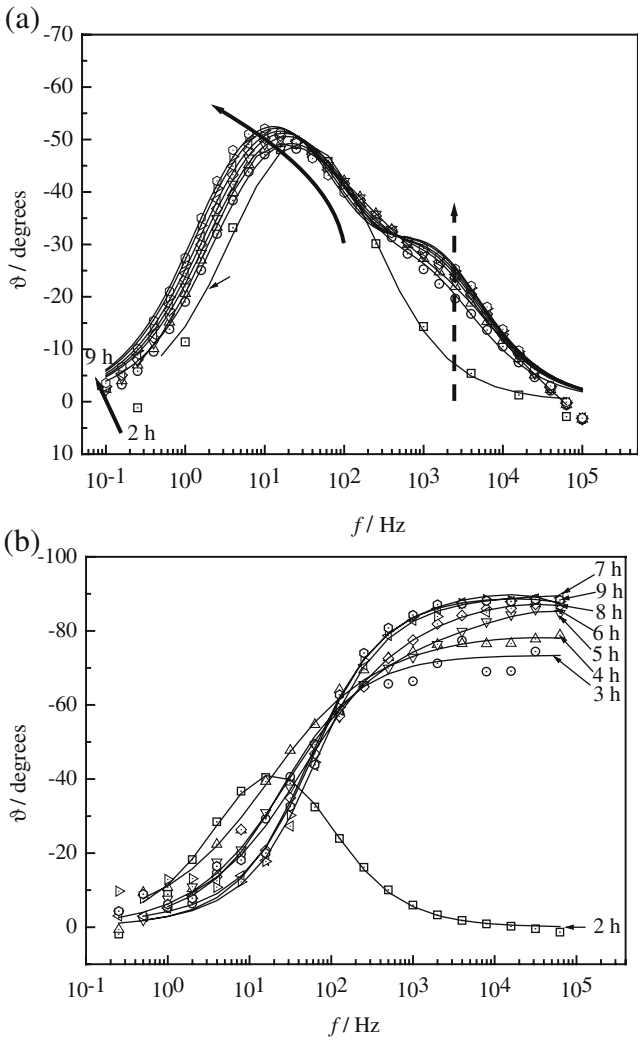

Fig. 14 Bode diagrams for carbon steel at different immersion times in inhibited 3% NaCl solution using inhibitor AMEI-18: **a** without diesel and **b** with diesel. *Symbols* are experimental values, *solid lines* are the calculated values

Figure 14 shows the corresponding Bode plot for the same experimental data in the format θ vs log f for both solution tests. As in the case of inhibitors HEI-18 and AEI-18, the bode phase broadens at low frequencies but shows clearly resolved time constants at higher frequencies as time increases. Unlike the other inhibitors, two distinct time constants are present when the oily phase is absent, but the position of the peak at higher frequencies remained constant as time increased, and the peak at low frequencies is shifted towards low frequencies as the immersion time increases. When diesel is added, the peaks remain constant as time elapses. The fitting of curves are shown in Fig. 13a,b and Fig. 14a,b as solid lines for each spectrum, observing an optimum fit with the model for all experimental data, with an estimated error of 3% in all cases.

From Table 5 we can see that, when diesel is absent, the calculated proportional factor Y of CPE increases with time, and this increase has been related to the growing area of an iron carbonate deposit on the surface of the samples [16]. At 50 °C these scales are porous and nonhomogeneous, allowing the access of the corroding solution to the base material. These scales, however, seem to provide some corrosion protection to the metal beneath them by restricting the mass transfer of reactants and products between the bulk solution and the metal, which is represented by an increase in the corresponding R_{ct} values. On the other hand, there is no evidence of the formation of a protective $FeCO_3$ film because there is only one capacitive loop in the EIS Nyquist plots [16]. This could be due to the formation of a porous thin layer of $FeCO_3$ with a resistance that is much smaller than the charge transfer resistance, R_{ct}, which can be seen in Figs. 15 and 16. In Fig. 15, the change on the film resistance for the inhibited 3% NaCl solution without and with diesel is shown. On the other hand, Fig. 16 shows the calculated charge transfer resistance for these solutions. It can be seen that, when diesel is present, both R_f and R_{ct} had maximum values for inhibitor HEI-18I, which provided the highest corrosion protection efficiency. The semicircle representing

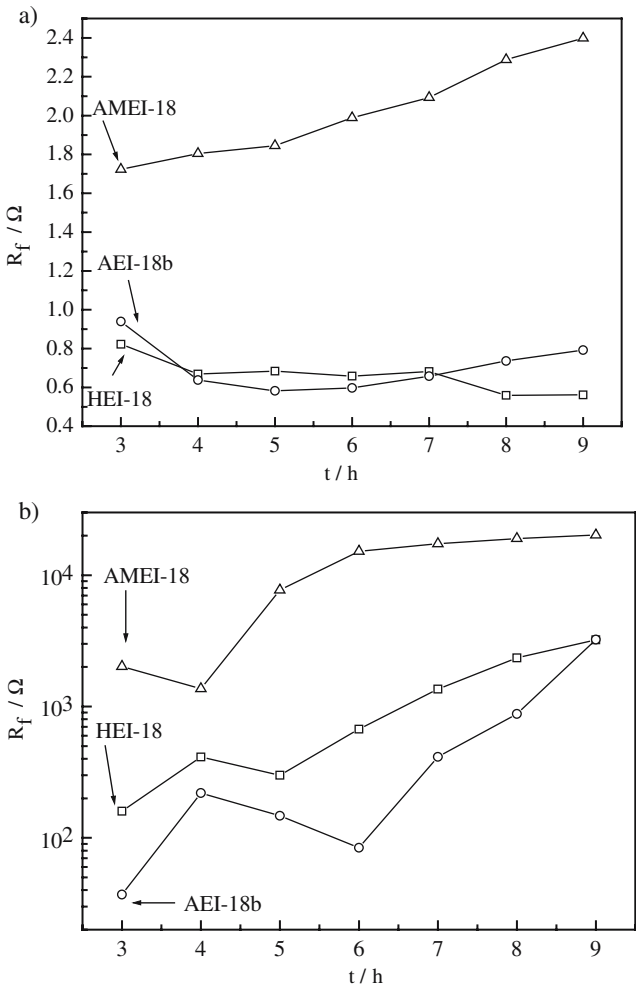

Fig. 15 Change in the film resistance value, R_f, with time for the different imidazolines in **a** 3% NaCl and **b** 3% NaCl+diesel solutions

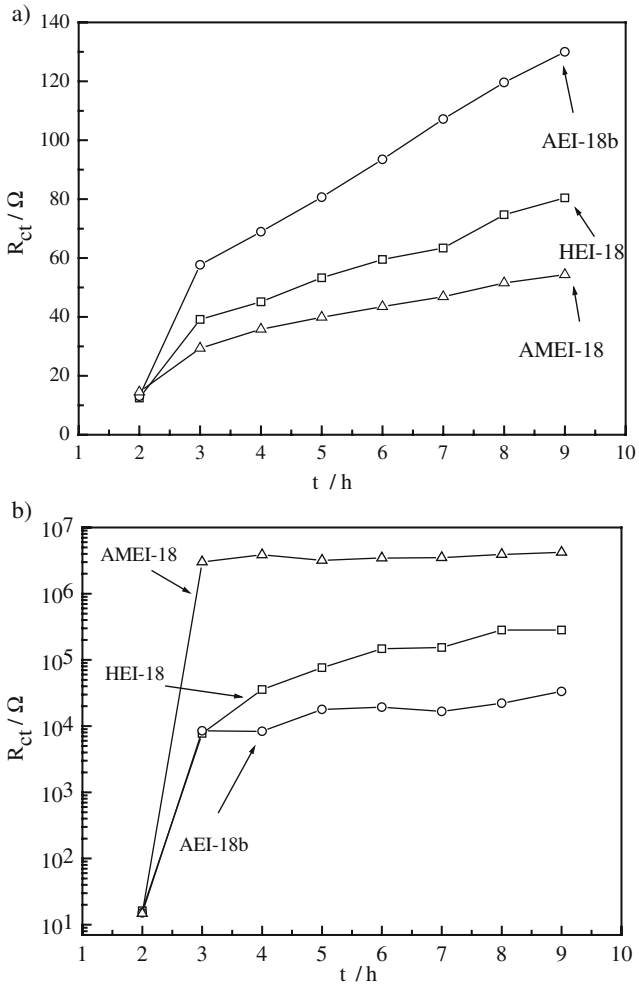

Fig. 16 Change in the charge transfer resistance value, R_{ct}, with time for the different imidazolines in **a** 3% NaCl and **b** 3% NaCl+diesel solutions

the $FeCO_3$ film emerges with the charge transfer loop, and hence, the EIS data are described by a simple capacitive semicircle [17].

On the other hand, from Table 6, the calculated proportional factor *Y* of CPE for the 3% NaCl+diesel solution decreases with time, which could be related to the formation of a protective, not porous, $FeCO_3$ layer. Even more, the charge transfer resistance value for the 3% NaCl solution increased with time, indicating that the corrosion rate slowly decreases, whereas the same value for the 3% NaCl+diesel solution is almost kept unchanged from the very beginning, indicating that the formed film starts to protect against corrosion almost immediately.

Conclusions

In 3% NaCl solutions, the corrosion rate decreased with the addition of hydroxyethyl, amino ethyl, and amidoethyl imidazolines inhibitors, but the time to reach a steady state was much longer than when diesel was added. The relative efficiencies of the three compounds studied in deaerated 3% NaCl+diesel solutions at 50 °C were found to be in the following order: amidoethyl imidazoline>aminoethyl imidazoline>hydroxyethyl imidazoline.

When diesel and inhibitors were present, the formed film was much more stable, not porous, avoiding the contact of the electrolyte and the underlying metal. The film formed with the amidoethyl imidazoline inhibitor was much more stable as soon as it was added to the solution, but for the hydroxyethyl and aminoethyl imidazoline inhibitors, the stability of the film improved as time elapsed.

References

1. Kermani MB, Morshed A (2003) Corrosion 59:659
2. Jovancicevic V, Ramachandran S, Prince P (1999) Corrosion 55:449
3. Ramachandran S, Jovancicevic V (1999) Corrosion 55:259
4. Xueyuan Z (2001) Corros Sci 43:1417
5. Bentiss F, Lagrenee M, Traisnel M, Hornez JC (1999) Corros Sci 41:789
6. Bentiss F, Traisnel M, Lagrenee M (2001) J Appl Electrochem 31:449
7. Jovancicevic V, Ramachandran S, Prince P (1999) Corrosion 55:449
8. Ramachandran S, Tsai M, Blanco M, Chen H, Tang WA (1999) Langmuir 12:6419
9. Wang D, Ying S, Li M, Wang M, Xiao Z, Chen Z (1999) Corros Sci 49:911
10. Cruz J, Martinez-Aguilera LMR, Salcedo R, Castro M (2001) Int J Quant Chem 85:1911
11. Cruz J, Martinez R, Genesca J, Garcia-Ochoa E (2004) J Electroanal Chem 566:111
12. Rodriguez-Valdez LM, Martinez-Villafañe A, Glossman-Mitnik D (2004) Theochem 681:83
13. Rodriguez-Valdez LM, Martinez-Villafañe A, Glossman-Mitnik D (2005) Theochem 713:65
14. Bilkova K, Hackerman N, Bartos M (2002) In: Proceedings of NACE Corrosion/2002, Denver, CO
15. Macdonald JR (1987) J Electroanal Chem 223:25
16. de Morales FD, Shadley JR, Chen J, Rybicki E (2000) In: Proceedings of the NACE Corrosion/2000, Orlando, FL
17. Walter GW (1989) Corros Sci 26:681